Electric polarization properties of single bacteria measured with electrostatic force microscopy

Theoretical and practical studies of Dielectric constant of single bacteria and smaller elements

Daniel Esteban i Ferrer

UNIVERSITAT DE BARCELONA

Electric polarization properties of single bacteria measured with electrostatic force microscopy

Theoretical and practical studies of Dielectric constant of single bacteria and smaller elements

Daniel Esteban i Ferrer

Barcelona, September 2014

DOCTORAL THESIS

7 Dielectric characterization of single bacteria using Electrostatic Force Microscopy

7.1 Abstract

We quantified the electrical polarization properties of single bacterial cells using electrostatic force microscopy. We found that the effective dielectric constant, $\varepsilon_{r,eff}$, for the four bacterial types investigated (*S. typhimurium*, *E. coli*, *L. sakei* and L. *innocua*) is around 3-5 under dry air conditions. Under ambient humidity, it increases to $\varepsilon_{r,eff}$ ~ 6-7 for the Gram-negative bacterial types (*S. typhimurium*, *E. coli*) and to $\varepsilon_{r,eff}$ ~15-20 for the Gram-positive ones (*L. sakei* and L. *innocua*). We show that the measured effective dielectric constants can be consistently interpreted in terms of the electric polarization properties of the biochemical components of the bacterial cell compartments and of their hydration state. These results demonstrate the feasibility of label-free electrical studies of single bacterial cells.

7.2 Introduction

The response of bacterial cells to external electric fields has previously been investigated using a variety of spectroscopic techniques, such as dielectric impedance spectroscopy [39], dielectrophoresis spectroscopy [40] and electrorotation spectroscopy [41]. These studies have revealed that the electrical response of bacteria depends on their shape and size, their internal structure, and the electric conductivity and permittivity of the different bacterial cell components, which may

depend on the bacterial physiological state. Based on these results, the internal structure of a bacterial cell was inferred [42] and a number of electrical technologies were developed, including those to detect pathogenic bacteria [43] to detect the presence of bacterial cells [44], to count and differentiate bacteria [45], to determine bacterial viability [46], to distinguish among isogenic mutants [47] and to separate bacteria from other cell sources [48].

Most previous studies of the electrical properties of bacterial cells were carried out on bacterial populations of millions of cells. Only in the cases of electrorotation [41] and impedance cytometry [45] were single bacteria electrical measurements reported, but these had limited sensitivity and were based on complex electro-optical set-ups. Single cell measurements allow one to assess heterogeneity within a population and to perform measurements from a mixed sample without the need for separations. Recently, we demonstrated that electrostatic force microscopy (EFM) can be used to quantify the electrical properties of three-dimensionalnano-objects, like nanoparticles and viruses, with high accuracy and reliability [29]. This technique therefore is an ideal candidate to address the study of the electrical properties of single bacterial cells.

Herein we show that electrostatic force microscopy (EFM) can be used to quantify the electric polarization response of single bacterial cells with high accuracy and reproducibility. We measured four bacterial cell types (*Salmonella* typhimurium, *Escherichia coli*, *Lactobacillus sakei*, and *Listeria innocua*), two of them Gram-negative (*S. typhimurium* and *E. coli*) and two Gram-positive (*L.innocua* and *L. sakei*), in two environmental conditions, dry air (room temperature and < 1% relative humidity (RH)) and ambient conditions (room temperature and > 30% RH). We show that the effective dielectric constants obtained for the different bacterial types are well correlated with the intrinsic electric polarization properties of the biomolecular constituents and the hydration state of bacteria, thus opening interesting possibilities for further label-free analytical studies of single bacteria.

7.3 Results and discussion

We measured the effective dielectric constant of single bacterial cells with EFM following the procedure recently developed for nanoparticles and single viruses [29], as outlined schematically in Figure 7.1. Briefly, the electric polarization force between a bacterium and a nanometric conducting tip mounted on a force-sensing cantilever was measured at different positions while an alternating electric potential was applied between the tip and the underlying substrate.

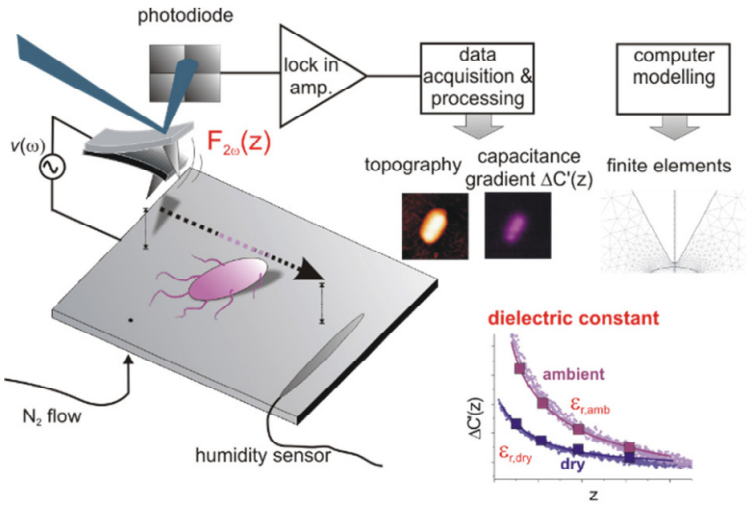

Figure 7.1 *Schematic of measurement of the effective dielectric constant of a single bacterium using electrostatic force microscopy. Polarization force approach curves were obtained for each bacterium. The geometry of the bacterium was obtained from the topographic image. Finite element numerical simulations of a homogeneous bacterium using the calibrated geometry of the probe were used to fit the experimental results and obtain the effective dielectric constant of the cell.*

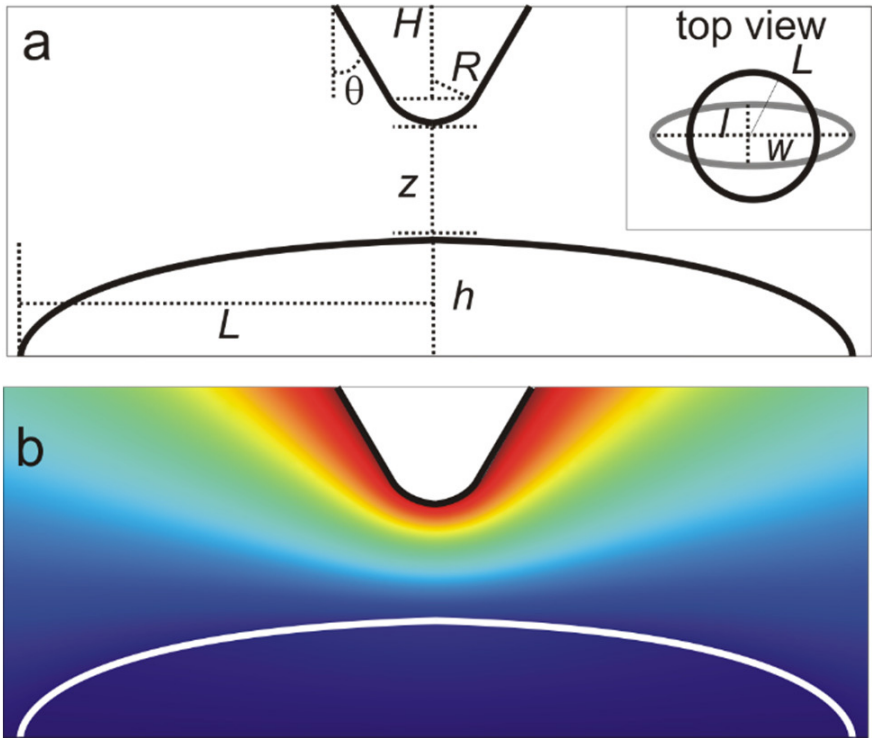

Figure 7.2 *(a) Schematic representation of the tip sample system used in the finite element numerical calculations with the different input parameters indicated (drawing not to scale). The inset represents the top view with the solid line showing the axisymmetric model that preserves the volume of the bacterium (thin line). (b) Example of a voltage distribution obtained for the case of a 200 nm high and 1.4 µm wide bacterial cell modelled as a solid oblate hemispheroid with effective dielectric constant er,eff = 6. NB: only part of the domain of simulation is shown.*

The dielectric constant was obtained by matching the experimental polarization force to that from a theoretical model in which the electrical properties of the bacterium were the changeable parameters. The model takes into account the sample and the probe geometries, which are obtained from topographic images and a tip calibration procedure, respectively (see Figure 7.2 and Ref. [29] and [30] for details).

Figure 7.3 shows the results of measurements performed on a single *S.* typhimurium cell in ambient conditions. The topographic image of the bacterium (Figure 7.3a) reveals the physical dimensions of this particular cell as: l = 2 μm, w = 1 μm and h = 205 nm, as can be seen more clearly from cross section topographic profiles along the main axes of the bacterium (Figure 7.3b).

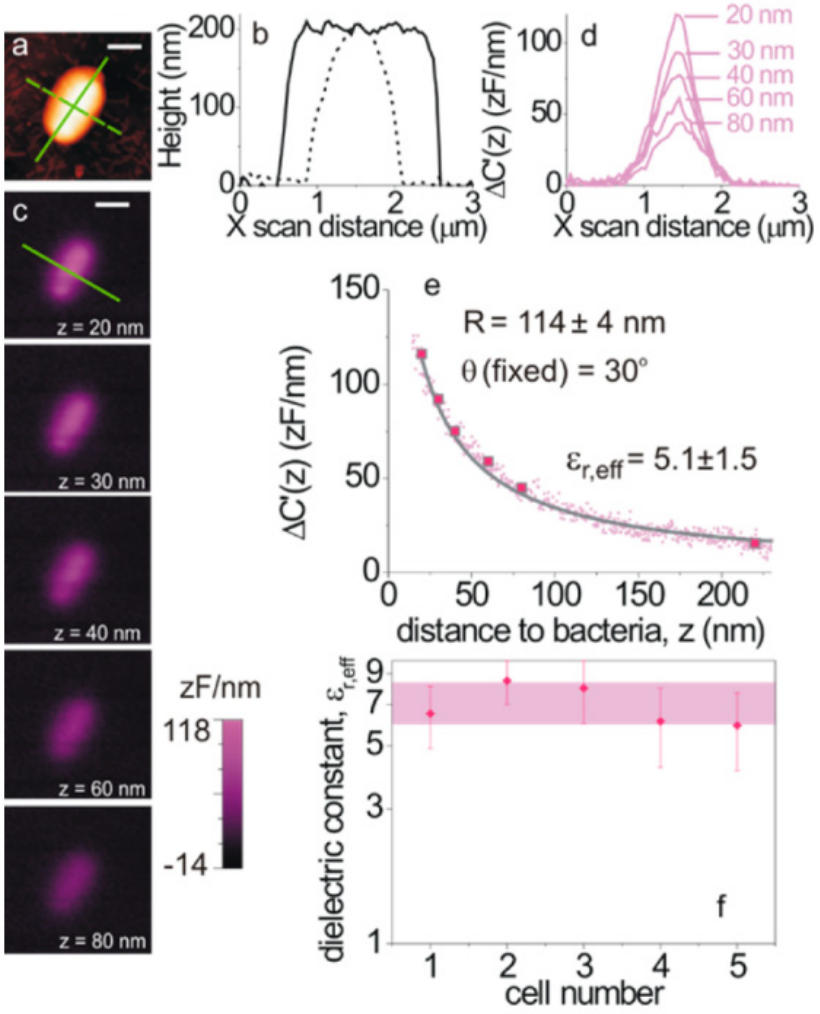

Figure 7.3 *Measurement of the dielectric constant of a single S. Typhimurium cell in ambient conditions. (a) Topography and*

(b) cross-section profiles of the cell analyzed. (c) Capacitance gradient images and (d) cross-section profiles measured at different scan distances from the bacterium z = 20, 30, 40, 60, 80 ± 2 nm. Scale bar: 680 nm. (e) Capacitance gradient contrast approach curves (N=12) measured on the centre of the cell (pink dots). The filled symbols correspond to the maximum electric contrast obtained from the dielectric images in (c). The solid dark grey line is the fitted numerical calculation giving a dielectric permittivity of 5.1 ± 1.5 using a calibrated tip radius of 114 ± 4 nm and a oblate hemispheroid with h = 205 nm and L= 1.41 µm (extracted from the measured w = 1 µm and l = 2 µm). (f) Dielectric constants measured on n = 5 different S. Typhimurium cells with different tips. The average value over the measured bacteria is r,eff = 7 ± 1.

Electric polarization force images (shown as capacitance gradient images) of the same bacterial cell taken at increasing distances from the bacterium are shown in Figure 7.3c. As can be seen, the electrostatic force images clearly detect the presence of the bacterium with a contrast that decreases as the tip-bacterium distance increases. This is clearly evident in Figure 7.3d, which shows electric profiles taken along cross-section of the cell indicated in the electric images in Figure 7.3c. The maximum contrast ranges from 116 zF/nm at z = 20 nm from the cell to 15 zF/nm at z = 230 nm.

These maximal dielectric contrast values as a function of distance are shown in Figure 7.3e as large squares. They were obtained by averaging the value of the electric signal on few pixels around the electric maximum and subtracting it from the value obtained by averaging the values in the same number of pixels on the electrode substrate. Note that the noise level of the measuring instrument is about ± 5 zF/nm, thus giving an excellent signal to noise ratio in all cases. Figure 7.3e also shows contrast approach curves measured above the center of the bacteria (small dots corresponding to N = 12 curves). These curves agree with the dielectric contrast approach curves obtained from the dielectric images, thus validating the reliability and reproducibility of the dielectric measurements based on approach curves taken on the bacterial cell.

The solid line in Figure 7.3e represents the best-fit numerically calculated dielectric contrast curve, using R = 114 ± 4 nm, calculated as detailed in Methods bacterial dimensions derived from the topography and $\varepsilon_{r,eff}$ as the only variable. For these data the best fit value was $\varepsilon_{r,eff} \sim 5.1 \pm 1.5$ where the uncertainty arises due to instrumental noise.

Figure 7.3f summarizes the values of $\varepsilon_{r,eff}$ as determined for five additional *S.* Typhimurium cells using different tips. While the geometric parameters varied (R = 81-160 nm, h = 180-250 nm), the extracted dielectric constants lie in a narrow range of values for all the samples, thus we can say that the effective dielectric constant is an intrinsic property of the bacterial cell and that for *S. Typhimurium* in ambient conditions it has a value $\varepsilon_{r,eff} = 7 \pm 1$ (error represents 1 standard deviation of the mean; for full details of all geometric parameters see Sec. 4 of the Appendix).

The same measurement procedure was repeated with the other cells (n = 5), the results of which are summarized in Table 1 (additional plots and geometric data and dielectric constant of each cell are reported in Secs. 7.6.3, 7.6.4).

TABLE 1. Measured Mean Dielectric Constants of the Four Bacterial Types Analyzed in Ambient and Dry Conditions and Obtained from *n* = 5 Different Bacterial Cells in Each Case, Together with Its Mean Geometric Parameters (height and mean effective equatorial radius)

bacteria	Gram	$\varepsilon_{r,eff,amb}$	$\varepsilon_{r,eff,dry}$	*h* /nm	*L* /μm
S. typhimurium	−	7 ± 1	4.7 ± 1	212 ± 26	0.75 ± 0.06
E. coli	−	6.5 ± 1	3.3 ± 0.4	348 ± 34	0.9 ± 0.1
L. sakei	+	19 ± 5	3.3 ± 0.6	636 ± 40	1.1 ± 0.1
L. innocua	+	18 ± 7	3.7 ± 0.7	260 ± 33	0.7 ± 0.1

In ambient conditions a strong correlation of the dielectric constant with the Gram-type is observed; namely, the Gram-positive bacteria (*L. sakei*, *L. innocua*) show relatively large values ($\varepsilon_{r,eff} \sim 18$ - 19) while the Gram-negative bacteria (*S.* typhimurium, *E. coli*) show much smaller values $\varepsilon_{r,eff} \sim 6$ - 7. Furthermore, we note that within the Gram-type, different bacteria show remarkably similar values of dielectric constant, thus indicating a relatively small dependence on the

bacterial type. While the absolute error for *L. sakei* and *L. innocua* is higher than that for the *S.* typhimurium and *E. coli*, the relative error is similar ($\sim$ 25%) because it is associated with the measurement error sources which are the same in both cases.

We next addressed the effect of relative humidity of the measured effective dielectric constant by reducing the humidity in the environmental chamber to a dry condition (<1% RH) and remeasuring the same cells. The values of the dielectric constants obtained under dry conditions are shown in Table 1 and as gray symbols in Figure 7.4a whereas the cyan symbols represent the effective dielectric constants of the same cells measured under ambient conditions. The error bar represents the standard deviation over a set of N =10 - 15 force curves measured on each bacterium. The colored bands are centered on the mean value for each bacterial type and their width represent plus minus one standard deviation which is also reported in Table 1. The effective dielectric coefficients measured in dry air conditions, $\varepsilon_{r,eff,dry}$, are significantly lower than those of the same bacteria measured in ambient conditions, $\varepsilon_{r,eff,amb}$. The change cannot be attributed to a change in the bacterial geometry, which remained unaltered, or to any significant effect of humidity in the tip radius which did not change (see section 7.6.5). We therefore attribute the observed reduction in the dielectric constant upon drying to a modfication of the dielectric properties of the bacterial cell itself.

We verified that these results were reversible for hydration/dehydration cycles as is shown in Figure 7.4b, where we plot the time evolution of the dielectric constants measured on a bacterium of each type when the environmental conditions were changed from ambient conditions to dry conditions (10 min) and back to ambient conditions (20 min).

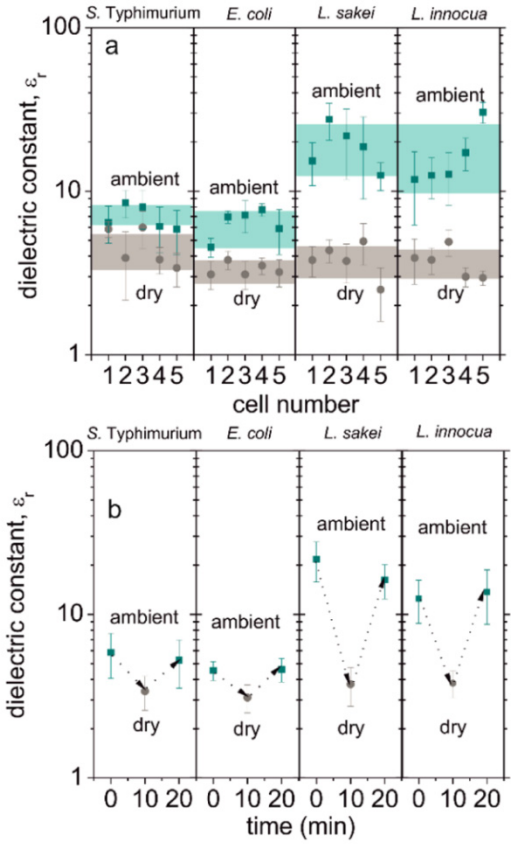

Figure 7.4 *Measured mean dielectric constants of four types of bacterial cells analyzed in ambient (30 - 40% relative humidity, cyan squares) and dry air (<1% relative humidity, gray circles) conditions. Each of the n = 5 bacterial cells was measured in both conditions. The dielectric constant significantly reduces upon drying with a larger reduction for the case of Gram-positive bacteria. The color-coded regions indicate the obtained standard deviation of the values for each bacterium type under the different conditions (cyan for ambient and gray for dry conditions). (b) Evolution of the dielectric constant of single bacterial cells in a hydration/dehydration/rehydration cycle, analyzed for a single bacterium of each type.*

The effective dielectric constant reported for each bacterial type, $\varepsilon_{r,eff}$, represents the electric polarization response of the whole cell under the influence of the external electric field generated by the sharp biased metallic probe. We consider the relationship of this parameter to the intrinsic dielectric constants of the different cell components using a simple core - shell model (see inset in Figure 7.5a for geometry), in which the core represents the cytoplasm region and the shell the bacterial envelope (which includes the plasma membrane, the cell wall, the periplasmic space, and, in the case of Gram-negative bacteria, the outer membrane).

We first note that the value of $\varepsilon_{r,eff}$ measured with EFM differs in general from the effective dielectric constant that would be obtained by considering an isolated core - shell bacteria in an uniform external electric field [49] (see section 7.6.6). In our previous work with very small core - shell objects like viruses of $\sim$ 60 nm in diameter, the electric field was approximately uniform for the entirety of object and analytical models for uniform external electric fields could be used [29]. However, for a larger object like a bacterial cell, this is not the case and we must use numerical calculations to investigate the relation between $\varepsilon_{r,eff}$ and the dielectric constants of the cell components and its geometry.

In the core - shell bacterial model, the total thickness of the envelope of a Gram-negative bacteria was taken to be δ = 25 nm, which lies within the characteristic range of values (20 - 30 nm), which includes the cell wall (2 - 7 nm thick), the outer membrane (7 - 8 nm), the periplasmic space (2 - 4 nm), and the cytoplasmatic membrane (7 - 8 nm). We did not include the external lipopolysaccharide chains, since they most probably disappeared during the sample preparation process.

The thickness of the envelope of the Gram-positive bacteria was taken to be δ = 65 nm, which is within the range of characteristic thicknesses for this type of bacteria (30 - 90 nm), which includes a much thicker cell wall (20 - 80 nm thick) but no outer membrane. Different dielectric constants were assigned to the shell and core, $\varepsilon_{r,shell}$ and $\varepsilon_{r,core}$ respectively, in order to account for a possible difference in their electric polarization response arising from their different biochemical composition.

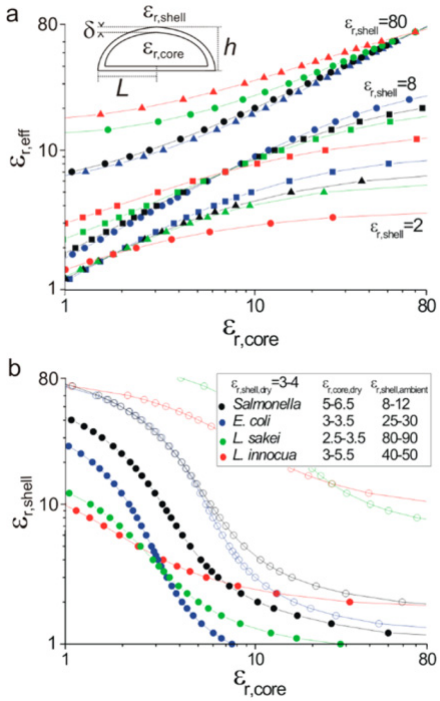

Figure 7.5 *(a) Effective dielectric constant of a core - shell bacteria model for the four bacteria types investigated: S. typhimurium (black symbols), E. coli (blue symbols), L. sakei (green symbols), and L. innocua (red symbols) as a function of the dielectric constant of the core for three di ff erent dielectric constants of the shell, $\varepsilon_{r,shell}$ = 2, 8, and 80. The dimensions of the bacteria correspond to the mean values reported in Table 1. The thickness of the shell for the Gram-negative bacteria is 25 nm, and for the Gram-positive, 60 nm. The tip radius is R = 100 nm, and the tip sample distance z = 20 nm. (b) Couples of values for $\varepsilon_{r,core}$ and $\varepsilon_{r,shell}$ compatible with the measured effective dielectric constants, $\varepsilon_{r,eff}$, for each bacterial type, in both dry (solid symbols) and ambient (empty symbols) conditions. Inset: Range of values for $\varepsilon_{r,core,dry}$ by assuming $\varepsilon_{r,shell,dry}$ = 3 - 4, and range of values of $\varepsilon_{r,shell,ambient}$ by assuming $\varepsilon_{r,core,ambient}$ = $\varepsilon_{r,core,dry}$.*

The bacterial sizes were taken as the mean values measured from the topography as reported in Table 1. The tip sample distance was taken as z = 20 nm and the probe radius R = 100 nm (the results are

insensitive to these parameters; see section S7 in Supporting Information). Figure 7.5a shows the dependence of $\varepsilon_{r,eff}$ for the four bacteria types investigated as a function of $\varepsilon_{r,core}$ for three characteristic values of $\varepsilon_{r,shell}$ = 2, 8, and 80.

In all cases, for a given $\varepsilon_{r,shell}$, the effective dielectric constant, $\varepsilon_{r,eff}$, increases with increasing $\varepsilon_{r,core}$ until a value of around 10 times $\varepsilon_{r,shell}$, at which it plateaus. This shows that $\varepsilon_{r,eff}$ includes contributions from both the envelope and the core of the bacterium, which is due to the long-range nature of the electrostatic forces. This is an important result, since it shows that although atomic force microscopy (AFM) is typically viewed as a surface technique, EFM is sensitive to the subsurface electric properties of the samples, in this case, the dielectric constant of the cytoplasm. We also note that for given $\varepsilon_{r,shell}$ and $\varepsilon_{r,core}$ the $\varepsilon_{r,eff}$ depends on the dimensions of the bacteria. These results show that $\varepsilon_{r,eff}$ depends on both the dimensions/structure of the bacterium and the dielectric properties of its constituent parts. Further simulations, where the probe dimensions and the tip - sample distance were varied over the range considered in this paper (R = 50 - 200 nm, z = 20 - 100 nm), determined that the calculated value of $\varepsilon_{r,eff}$ is independent of probe dimensions and it depends only weakly on the tip - sample distance (see section 7.6.7 for supporting data). Thus, $\varepsilon_{r,eff}$ can be considered an intrinsic parameter of the bacterium representing its effective electric polarization response, which includes both the electric polarization properties of the biochemical constituents and its geometry/internal structure.

For a fixed $\varepsilon_{r,eff}$ and geometry, there is a continuum possible of pairs of ($\varepsilon_{r,shell}$, $\varepsilon_{r,core}$) that would give rise to identical responses. Figure 7.5b shows sets of these pairs satisfying the experimentally measured $\varepsilon_{r,eff}$ for the four bacterial types and the two environmental conditions. As can be seen, there are a wide range of possible values for the core and shell dielectric constant that are compatible with the measured effective dielectric constants. However, in practice, this range can be reduced. In particular, we know that the envelope is mainly composed of proteins, lipids, and peptidoglycan, and that all these biomolecules are expected to show low electric polarization properties under dry conditions (around $\sim$ 2 for lipids [50] and $\sim$ 2 - 5 for proteins [51], [52]).

Therefore, a reasonable value for the shell dielectric constant under dry conditions can be chosen to be $\varepsilon_{r,shell,dry} \sim 3 – 4$ [52]. Assuming this range of values for the shell under dry conditions, the corresponding dielectric constants for the cytoplasm are in the ranges $\varepsilon_{r,core,dry} \sim 5$ - 6.5, 3 - 3.5, 2.5 - 3.5, and 3 - 5.5, for *S.* typhimurium, *E. coli*, *L. sakei*, and *L. innocua*, respectively. These values agree with the expected dielectric constants of the cytoplasm constituents ($\sim$ 2 - 5 for proteins and $\sim$ 8 - 12 for nucleic acids [29], [52]) and their relative proportions (roughly 3:1 proteins/nucleic acids dry weight).

Since the size of the bacterial cells did not change appreciably between the two environmental conditions, we assume that the cytoplasm remains unchanged and thus the dielectric constants of the core under ambient conditions are the same as those obtained from the analysis of the dry bacterial cells. Using these values, we obtain the dielectric constants for the shell in ambient conditions: $\varepsilon_{r,shell,ambient} \sim 8$ - 12, 25 - 30, 80 - 90, and 40 - 50, for *S.* typhimurium, *E. coli*, *L. sakei*, and *L. innocua*, respectively. In all cases, we observe that the shell dielectric constants in ambient conditions are larger than the corresponding ones in dry conditions and are significantly larger than those assigned to the biomolecular constituents ($\sim$ 2 for lipids and $\sim$ 2 - 5 for proteins).

These data suggest that the environmental humidity affects the dielectric response of the shell and that Gram-negative bacteria *S.* typhimurium and *E. coli* are less sensitive to changes in environmental humidity than the Gram-positive bacteria *L. sakei* and *L. innocua*. Structural differences between Gram-positive and Gram-negative bacteria that could cause this effect are (i) the presence of an outer membrane in Gram- negative cells, and (ii) the much thicker peptydoglycan layer in the Gram-positive bacteria. The outer membrane of Gram-negative bacteria is well-known as a permeability barrier for both hydrophobic and hydrophilic compounds. Nevertheless, it is considered that in bacterial cells the water permeability of bacterial membranes is high enough as to not require the presence of aquaporins for water transport [53]. Hence, we speculate that the hydration/dehydration of the multilayered peptidoglycan of *L. sakei* and *L. innocua* cells might account for the significant alteration of the

dielectric constant of their shells when the environmental humidity is modified.

We cannot rule out, however, that this effect might also be the consequence of a global hydrophobic/hydrophilic difference between both types of cells. We remark that measuring the hydrophobic or hydrophilic nature of bacterial surfaces is of importance in the understanding of a number of biological processes, including adhesion, and that the molecular basis for the different behavior of Gram-positive and Gram-negative bacteria remains to be determined. Measuring the dielectric constant of bacterial cells using the approach outlined in this work, including assessing their response to the environment humidity, is therefore a promising route to evaluate critical biological properties of bacterial cells, such as adhesion, virulence, or viability.

Finally, we note that the dielectric constant values obtained for the bacterial envelope in ambient conditions are close to the values usually reported from measurements performed in liquid media by means of different macroscopic dielectric characterization techniques (refs. [39] [41] and [54]). These values are in the order of $\sim$ 60 for the periplasm and $\sim$ 5 - 10 for the inner membrane and $\sim$ 10 for the outer membrane (when present). This indicates that in dielectric measurements performed in fully hydrated bacteria water contributes significantly to the dielectric response and masks the intrinsic dielectric response from the biomolecular constituents. From an analytical point of view, therefore, using dry conditions offers the advantage to get rid of the effects of water in the dielectric characterization of bacterial cells, and to have direct access to the intrinsic electric polarization properties of biochemical constituents.

7.4 Conclusions

In this work we have shown that electrostatic force microscopy can be used to measure the electric polarization properties of single bacterial cells in dry and ambient conditions. The effective dielectric constants of the cells obtained by assuming a homogeneous bacterial model revealed similar dielectric constants for the Gram-positive and Gram-negative bacteria in dry air conditions, $\varepsilon_{r,eff}$ ~ 3-5. Under ambient conditions larger values were systematically obtained for both groups, however the increase was much larger for Gram-positive bacteria ($\varepsilon_{r,eff}$~18-19) as compared to Gram-negative bacteria ($\varepsilon_{r,eff}$~6-7). Analysis of the results obtained with a core-shell model revealed that the effective dielectric constant values obtained in dry air conditions are consistent with the dielectric response expected from its biochemical constituents (lipids, proteins, and nucleic acids) in dry conditions. In ambient conditions the dielectric constant of the envelope significantly increases with respect to the dry values to $\varepsilon_{r,shell}$ ~ 10-30 and $\varepsilon_{r,shell}$ ~ 40-80 for the Gram-negative and Gram-positive bacteria, respectively. This change points towards a significant contribution of moisture, which has a larger impact in the Gram-positive than in the Gram-negative bacteria due to the thicker and more hydrophilic nature of their envelope. This work confirms that dielectric measurements of single bacterial cells can be correlated with the electric polarization response of their biochemical constituents and their internal structure, thus opening interesting possibilities for label-free analytical studies based on the bacterial electric polarization properties.

7.5 Materials and methods

Electric Polarization Force Measurements. We measured the po larization force using dynamic EFM in amplitude detection [29]. Briefly, an ac voltage of amplitude, v_{ac} , and frequency, ω , was applied to the probe. The induced force oscillation at double the frequency, $F_{2\omega}$, was detected using a lock-in amplifier while taking dielectric images or approach curves (Figure 7.1). The capacitance gradient in the z-direction was then obtained using the relationship $C'(z) = 4F_{2\omega}(z)/v_{ac}^2$. The tip

distance from the substrate was obtained taking into account the simultaneously measured mean deflection. The tip - bacteria distance, z, was obtained by subtracting the bacteria height from the tip - substrate distance. Electrical force curves were also measured on the bare metallic substrate, and it is the capacitance gradient contrast curves calculated as $\Delta C'(z) = C'_{bact}(z) - C'_{metal}(z + h)$ that we report in this work, where h is the height measured at the center of the bacterial cell.

Measurements were performed with a commercial atomic force microscope (Nanosurf, S.L.) connected to an external lock-in amplifier (Anfatec). Measurements were performed in an environmental chamber (Nanosurf) with humidity monitored with a humidity sensor (Rotronic AG). For dry conditions (RH < 1%), humidity was lowered with a N_2 flow, ambient conditions typically ~ 30 - 40% RH, both at room temperature. We used highly doped diamond probes (CDT-FMR, Nanosensors) with a spring constant of ~ 2 - 9 N/m, resonance frequency of ~ 100 kHz, nominal radius of ~ 100 nm, and half-cone angle of 30^o. The spring constant for each tip was determined by the thermal noise method. The analysis of the data was performed using the WSxM software (Nanotec Electrónica S.L.) and custom analysis routines written in Matlab (The Mathworks, Inc.). Dielectric images were obtained with the built-in constant height mode of the AFM instrument. All data were obtained with v_{ac} = 5 V RMS at ω = 2 kHz. Images were obtained at a speed of 1 s/line and approach curves at a velocity of 0.6 μ m/s.

Finite-Element Numerical Calculations. The expected force acting on the probe was calculated as a function of the tip - sample separation, geometry, and electrical properties of the bacterium by solving Poisson's equation using the commercial finite-element package Comsol Multiphysics 3.4, resulting in theoretical contrast curves $\Delta C'(z,\varepsilon_r)$ as a function of the effective dielectric constant of the bacteria. As in our previous work [29], [30] the tip was modeled as a truncated cone of half angle, θ, with a hemispherical apex of radius, R, and cone height, H. The bacterial cell was modeled as an oblate hemispheroid with polar semiaxis (height), h, and equatorial semiaxis (half-width), L. The hemispheroid geometry was used instead of the full spheroid geometry because it better reproduced the geometry of the adsorbed bacterial

cells (see Figure 7.7). Moreover, a hemispheroid geometry was used instead of a (hemi)ellipsoid ((half)rod shape) geometry, as it is amenable to two-dimensional axisymmetric numerical routines and reduces the number of variables considered. However, for calculations with the tip above the center of the bacteria, the spheroid geometry resulted in almost identical forces to the ellipsoidal one (errors < 5%, data not shown), as long as the polar axis, h, is maintained and the equatorial axis of the hemispheroid, L, is taken so that the volume of the bacteria is preserved, i.e., $L = 1/2(lw)^{1/2}$, where l and w are the cell width and length, respectively. A schematic representation of the system modeled together with a distribution of calculated electric potential is shown in Figure 7.2. Unless otherwise stated, the bacterial cell was modeled as a solid with no internal structure and with a homogeneous effective dielectric constant, $\varepsilon_{r,eff}$, and no conductivity.

Dielectric Constant Extraction. The (effective) homogeneous dielectric constant of the corresponding bacterial cell, $\varepsilon_{r,eff}$, was determined from the experimental capacitance gradient contrast curves, $\Delta C_{exp}'(z)$, by following the procedure developed previously [29]. First, the apex radius of the measuring probe, R, was determined by fitting numerically calculated approach curves to the experimental curves on a metallic substrate. In the fitting, the cone height and cone angle were kept fixed to their nominal values, $\theta = 30^o$ and H = 15 μ m, respectively (example of calibration curves and their theoretical fits are given in the Figure 7.8). We found tip radii in the range 100 - 200 nm, consistent with their nominal values. Second, the bacterial cell geometry was determined from the AFM topographic image, from where its length, l, height, h, and width, w, were obtained and used to determine the equivalent oblate hemispheroid geometry used in the theoretical models. Finally, theoretical capacitance gradient contrast curves, $\Delta C'(z, \varepsilon_{r,eff}) = C'_{bact}(z, \varepsilon_{r,eff}) - C'_{metal}(z + h)$, were calculated for different values of $\varepsilon_{r,eff}$ for the previously determined bacterium and probe geometries. These curves were then fitted to the experimental curves with $\varepsilon_{r,eff}$ taken as that which best fit the experiments. For each bacterium, a number N = 10 - 15 of experimental curves taken on the central region of the bacterium surface were analyzed. The reported values for $\varepsilon_{r,eff}$

correspond to the mean and standard deviation of the extracted values for the different curves. The main sources of error in the extracted dielectric constants come from the instrumental noise and the variability observed in the acquisition of multiple curves on a spot on a nonideal surface such a bacteria surface.

Bacterial Models and Sample Preparation. Four model bacteria with rod shape and similar dimensions when growing in liquid media ($\sim$ 2 μ m - 1 μ m) were analyzed. As examples of Gram-negative bacteria, we selected the well-studied *E. coli* strain MG1655 and the related genus Salmonella (*S.* typhimurium strain SV5015), which is an aethiologic agent of various infectious diseases. As examples of Gram-positive bacteria, we selected *L. sakei* strain SK1 and *L. innocua*.

A single colony from an agar plate was used to inoculate a plastic tube containing 2.5 mL of either Luria - Bertani broth (LB) (*S.* typhimurium, *E. coli*, *L. innocua*) or MRS agar broth (*L. sakei*).

Cultures were incubated overnight in a 37^{o} C shaker at 250 rpm. Cells were pelleted by centrifugation and resuspended in 2.5 mL of Milli-Q (MQ) water by vortexing for 20 s. Then 100 μ L of the *S.* typhimurium or *E. coli* suspension was deposited on freshly cleaved highly oriented pyrolitic graphite (HOPG) 1 cm - 1 cm plate and left to dry in a fl ow hood. The sample was then rinsed five times with MQ water to remove any poorly adhered cells and left to dry. As the *L. sakei* and *L. innocua* cells adhered poorly, the samples were diluted 50-fold before depositing and the rinsing step was omitted. The HOPG substrate was attached to a 1.5 cm diameter magnet using silver paint, which was connected to the electrical ground of the atomic force microscope by a small wire.

The sample preparation was obtained after trial and error with different concentrations, mediums, cleaning procedures, vortexing, centrifugation, etc. After each different sample preparation optical images on an inverted reflection microscope (Olympus) were taken until the desired separation, and concentration was obtained. In Figure 7.6 there is an example of a good spread bacteria sample of *S.* typhimurium.

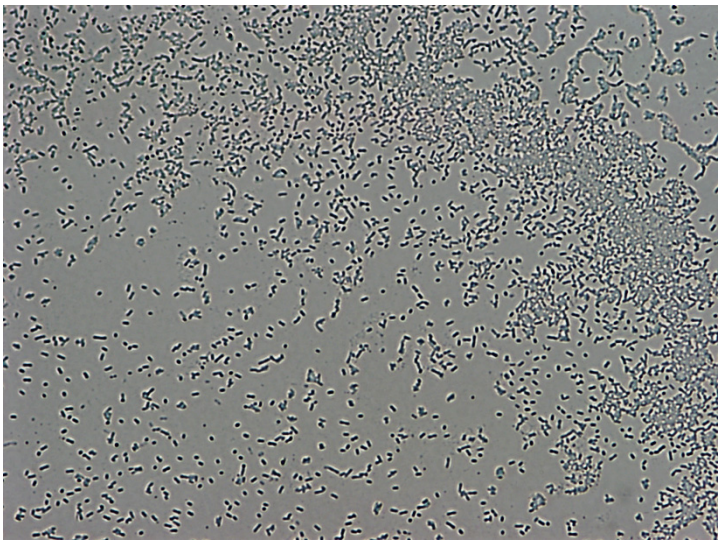

Figure 7.6 *Optical image of a good sample in concentration and spread of S.* typhimurium*.*

7.6 Appendix

7.6.1 Shape of the adsorbed bacteria

In Figure 7.7 we compare the experimental cross-sectional profile of two bacterial types (S. Typhimurium and *L. sakei*) with two possible geometries of the cells, namely hemi and full-ellipsoid geometries. As can be seen, the hemiellipsoid geometry is more compatible with the measured topography. While other geometries, like an ellipsoidalcap, could also be used to represent the profiles, for the sake of simplicity we have assumed a hemiellipsoidal shape, since it reproduces the experimental topography with sufficient accuracy, especially in the central part where electric measurements are performed.

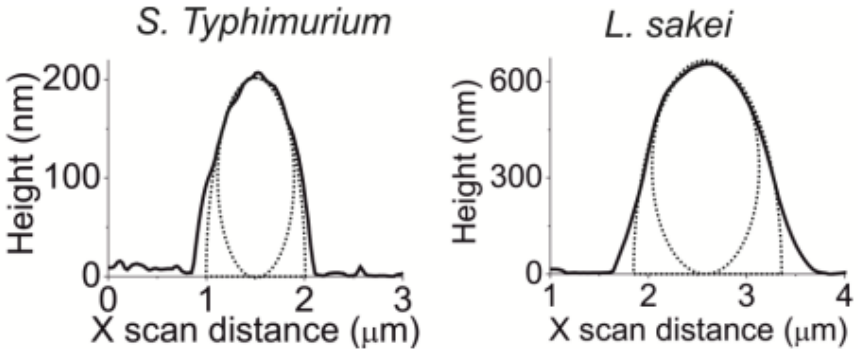

Figure 7.7 *Comparison of the measured topography (solid lines) with two possible bacteria geometries, hemiellipsoid and full ellipsoid geometries (dashed lines). In both cases, the hemiellipsoid geometry better reproduces the experimental topography.*

7.6.2 Tip radius calibration

The tip radius can be calibrated from electric force approach curves measured directly on a metallic substrate, as is detailed in our previous works [29] [30]. Two examples of electric force calibration curves and the corresponding fitted theoretical curves are shown in Figure 7.8 corresponding to the measurements shown in Figure 7.3 of the article and Figure 7.9 below, respectively. As can be seen the agreement between theoretical curves and experimental ones is excellent in the full range of distances considered. The fittings give tip radii R = 114 ± 4 nm and R = 124 ± 3 nm, respectively, with the cone semi-angle and cone height fixed to their nominal values θ = 30º and H = 15 μm.

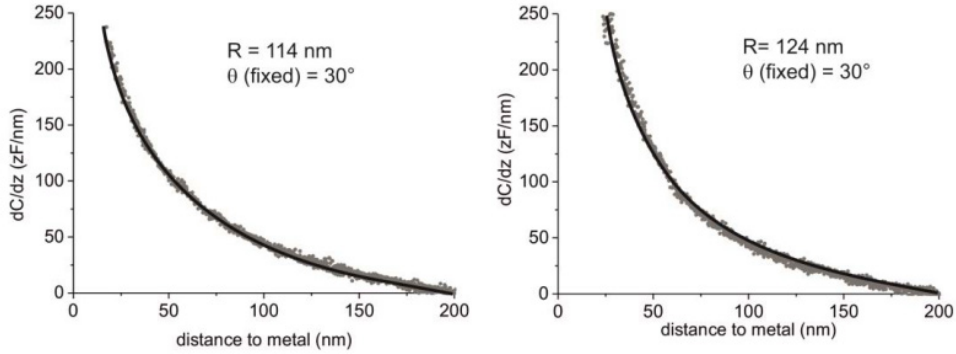

Figure 7.8 *Tip radius calibration in ambient conditions. Experimental capacitance gradient approach curves measured on a bare metallic substrate (symbols) and least square fitting of the theoretical model (continuous lines), with the apex radius as the only fitting parameter (the cone half angle and height were fixed to their nominal values, θ = 30º, H = 15 μm, respectively).*

7.6.3 Extraction of the dielectric constant of a single L. sakei cell in ambient conditions

Figure 7.9 show topographic and electrical measurements of a single *L. sakei* cell, as an additional example of the measurements shown in Figure 7.3 of the paper for the case of a *S.* Typhimurium cell. Figure 7.9a shows the topographic image. The height of the cell is 605 nm (Figure 7.9b), while the length and diameter were 1.5 μm and 2.1 μm, respectively. The dielectric images taken at different distances from the bacterium are shown in Figure S3c and the corresponding transversal profiles are given in Figure 7.9d.

Figure 7.9e shows the contrast approach curves (N = 11) taken at the center of the bacterium (violet dots) together with the maximum contrast measured from the dielectric images (blue squares), showing again a perfect match. Using the calibrated tip geometry R = 124 nm ± 3 nm (see the data of the calibration curve in section 7.6.2) and the measured geometry of the bacterium we obtain an effective dielectric constant of the bacterium of $\varepsilon_{r,eff} \sim 28 \pm 7$ (thick solid line in Figure 7.9e) where the error here represents the measurement standard deviation (as defined in the Materials and Methods section). Figure 7.9f summarizes the values of $\varepsilon_{r,eff}$ as determined for five additional cells using different tips. While the geometric parameters varied (R=107-170 nm, h=570-690 nm), the extracted dielectric constants lie in a narrow range of values for all the samples, thus we can say that the effective dielectric constant is an intrinsic property of the bacteria and that for *L. Sakei* in ambient conditions is has a value $\varepsilon_{r,eff} = 19 \pm 5$ (error represents 1 standard deviation of the mean; for full details of all geometric parameters see section 7.6.4).

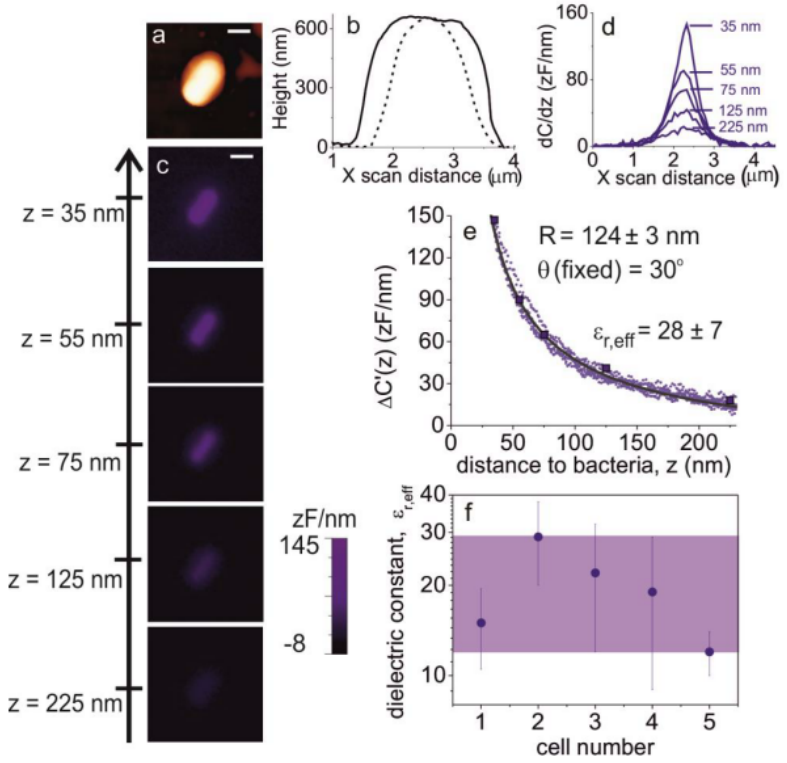

Figure 7.9 *Measurement of the dielectric constant of a single L. sakei cell. (a) Topography and (b) profile cross-sections of the bacterium analyzed. (c) Capacitance gradient images and (d) profile cross-sections measured at different scan distances from the cell z = 35, 55, 75, 125, 225 ± 2 nm. Scale bar: 960 nm. (e) Capacitance gradient contrast curves (N = 11) measured on the center of the cell (violet dots). The filled symbols correspond to the maximum electric contrast obtained from the dielectric images in (a). The solid dark blue line is the fitted numerical calculation giving a dielectric permittivity of* $\varepsilon_{r,eff}$ *=28 ± 7 using a calibrated tip radius of 124 ± 3 nm and a oblate hemispheroid with h = 600 nm and L = 1.75 mm (extracted from the measured topographic width and length w = 1.5 μm and l = 2.1 μm). (f) Dielectric constants measured on n=5 different L. sakei cells with different tips. The average value over the measured cells is* $\varepsilon_{r,eff}$ *= 19 ± 6.*

7.6.4 Data of the bacteria in Table 1 (ambient conditions)

The data of the individual bacterial cells corresponding to Table 1 are recorded in the tables below:

***S.*Typhimurium**	***l* / µm**	***w* /µm**	***h* / nm**	***L* / µm**	***R* / nm**	$\varepsilon_{r,eff}$
N1	2.6	1.1	170	0.85	160 ± 5	6.5 ± 1.6
N2	2.7	1	220	0.8	150 ± 4	8.5 ± 1.5
N3	1.9	1.1	200	0.7	105 ± 5	8 ± 2
N4	1.8	1	220	0.7	81 ± 3	6.1 ± 1.9
N5	1.7	1.2	250	0.7	91 ± 3	5.9 ± 1.8
AVERAGE	**2.1±0.4**	**1.1±0.1**	**212±26**	**0.75±0.06**	**117 ± 32**	**7 ± 1**

E. coli	***l* / µm**	***w* /µm**	***h* / nm**	***L* / µm**	***R* / nm**	$\varepsilon_{r,eff}$
N1	2.4	1.5	400	0.95	145 ± 4	4.5 ± 0.6
N2	1.9	1.3	370	0.8	134 ± 4	7 ± 0.6
N3	2.1	1.4	340	0.85	100 ± 4	7.2 ± 1.6
N4	2.5	1.5	300	0.95	112 ± 3	7.7 ± 0.7
N5	2.3	1.5	330	0.9	99 ± 4	5.9 ± 1.8
AVERAGE	**2.2±0.2**	**1.4±0.1**	**348±34**	**0.9±0.1**	**118 ± 18**	**6.5 ± 1.1**

L. sakei	***l* / µm**	***w* /µm**	***h* / nm**	***L* / µm**	***R* / nm**	$\varepsilon_{r,eff}$
N1	2.7	1.9	690	1.1	160 ± 5	15 ± 4.5
N2	2.7	1.8	650	1.1	140 ± 5	27 ± 7
N3	2.9	2	570	1.2	150 ± 4	22 ± 10
N4	2.3	1.7	620	1	170 ± 5	19 ± 10
N5	2.3	1.5	650	0.9	107 ± 3	12 ± 2
AVERAGE	**2.6±0.2**	**1.8±0.2**	**636±40**	**1.1±0.1**	**145 ± 22**	**19 ± 5**

L. innocua	*l* / µm	*w* /µm	*h* / nm	*L* / µm	*R* / nm	$\varepsilon_{r,eff}$
N1	1.7	1.1	280	0.7	103 ± 5	12 ± 6
N2	2.1	1.1	310	0.75	130 ± 4	12 ± 3.5
N3	2	1.1	250	0.75	150 ± 5	13 ± 4.5
N4	1.5	1	250	0.6	142 ± 3	17 ± 4
N5	2	1.3	210	0.8	123 ± 3	30 ± 4
AVERAGE	**1.9±0.2**	**1.1±0.1**	**260±33**	**0.7±0.1**	**130 ± 16**	**17 ± 7**

7.6.5 Effect of humidity on tip radius calibration

We verified that the change of the environmental conditions does not substantially affect the electrostatic force felt by the measuring probe. Figure 7.10 shows two calibration approach curves taken under dry and ambient conditions for two different probes. For the data on the left hand side plot we obtained tip radii of 81 nm in ambient conditions and 75 nm in dry conditions, while for the right hand side plot we obtained 124 nm in ambient conditions and 115 nm in dry conditions. As can be seen the effect of ambient humidity in tip radius calibration do not exceed 10%, which would only have a minor impact on the extracted dielectric constants.

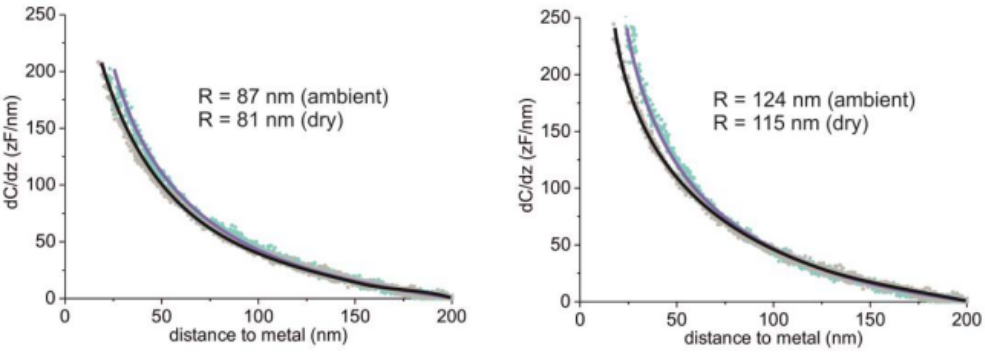

Figure 7.10 *Comparison of tip radius calibration in dry and ambient conditions. Experimental capacitance gradient approach curves measured on a bare metallic substrate (symbols) and least square fitting of the theoretical model (continuous lines), with the apex radius as the single fitting parameter (the cone half angle, and the microscopic probe geometry, were fixed to their nominal values, θ = 30º, H = 15 μm). Blue and gray symbols correspond to experimental data for ambient and dry conditions, respectively and the purple and black lines to their theoretical fits.*

7.6.6 Comparison of the effective dielectric constant of a core shell oblate spheroid in a uniform electric field and in the electric field created by an EFM tip

As discussed in Ref. [29], the effective dielectric constant of an oblate spheroid core-shell object in a uniform external electric field is given by [55]:

$$\varepsilon_{r,eff,k} = \varepsilon_{r,shell} \frac{\left[\left(\varepsilon_{r,core} - \varepsilon_{r,shell}\right) L_{ck} + \varepsilon_{r,shell}\right] + c\left(\varepsilon_{r,core} - \varepsilon_{r,shell}\right)\left(1 - L_{sk}\right)}{\left[\left(\varepsilon_{r,core} - \varepsilon_{r,shell}\right) L_{ck} + \varepsilon_{r,shell}\right] - c\left(\varepsilon_{r,core} - \varepsilon_{r,shell}\right) L_{sk}}; \qquad k = x, y, z \quad (7.1)$$

where $\varepsilon_{r,core}$ and $\varepsilon_{r,shell}$ are the relative dielectric constants of the core and shell, respectively, a_{ck} and a_{sk} (k = x, y, z) are the dimensions of the core and shell along the principal axes and $c = a_{cx}a_{cy}a_{cz}/a_{sx}a_{sy}a_{sz}$ is the volume fraction of the core. The geometrical factors L_{sk} and L_{ck} (k = x, y, z) are given by

$$L_{ck} = \frac{a_{cx}a_{cy}a_{cz}}{2}\int_0^\infty \frac{dt}{\left(a_{ck}^2+t\right)\sqrt{\left(a_{cx}^2+t\right)\left(a_{cy}^2+t\right)\left(a_{cz}^2+t\right)}}; \qquad k = x, y, z$$

(7.2)

$$L_{sk} = \frac{a_{sx}a_{sy}a_{sz}}{2}\int_0^\infty \frac{dt}{\left(a_{sk}^2+t\right)\sqrt{\left(a_{sx}^2+t\right)\left(a_{sy}^2+t\right)\left(a_{sz}^2+t\right)}}; \qquad k = x, y, z$$

(7.3)

For an oblate spheroid, that is $a_{cx} = a_{cy} \neq a_{cz}$ and $a_{sx} = a_{sy} \neq a_{sz}$, we have $L_{cx} = L_{cy} \neq L_{cz}$ and $L_{sx} = L_{sy} \neq L_{sz}$. Thus $\varepsilon_{r,eff,x} = \varepsilon_{r,eff,y} \neq \varepsilon_{r,eff,z}$ and the effective dielectric constant is anisotropic. In the experimental configuration of the article the electric field is applied along the z direction of the oblate spheroid bacteria. Hence, the effective dielectric constant measured corresponds to the z component of the dielectric constant of the effective uniform model (Eqs. (7.1),(7.2),(7.3)with k = z). In Figure 7.11 we show the dependence of $\varepsilon_{r,eff}$ on $\varepsilon_{r,core}$ and $\varepsilon_{r,shell}$ predicted by Eqs. (7.1),(7.2),(7.3)(continuous lines) and compare it with the one obtained from finite-element numerical calculations (dashed lines) for a bacterial model representative of *L. sakei*. For consistency with the theoretical derivation of Eqs. (7.1)-(7.3) that assumes a full spheroid model here we also considered a full spheroid model in the numerical calculations. Large discrepancies between the analytical model for a uniform electric field and the one corresponding to an EFM set up dictate that one cannot use the analytical model to interpret quantitatively EFM measurements on a core-shell bacteria model.

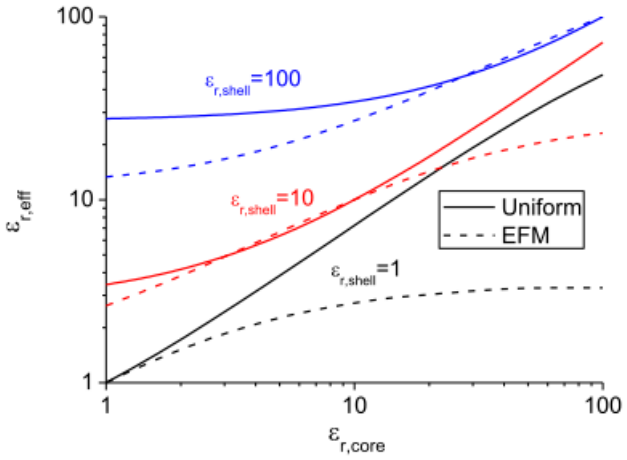

Figure 7.11 *Effective dielectric constant of a core-shell spheroid as a function of the dielectric constant of the core and for different dielectric constants of the shell. Continuous lines correspond to the case of a uniform electric field (Eqs. (7.1)-(7.3)) while the dashed lines correspond to the case of an electric field created by an EFM set up. Geometric parameters of the cell model correspond to the L. sakei cells ($a_{cx} = a_{cy}$ =1.04 μm ≠ a_{cz} =0.26 μm, and $a_{sx} = a_{sy}$ =1.1 μm ≠ a_{sz} =0.32 μm). Similar results are obtained for other bacterial models. Probe parameters: R=100 nm, θ=30º, H=15 μm and z=20 nm.*

7.6.7 Intrinsic nature of the effective dielectric constant measured by EFM

The effective dielectric constant defined in the manuscript is independent from the measuring radius of the tip and only depends slightly on the measuring distance, so that it can be considered an intrinsic dielectric parameter characterizing the dielectric response of the bacterium in EFM measurements. This is shown explicitly in Figure 7.12a where we show the dependence of $\varepsilon_{r,eff}$ on $\varepsilon_{r,core}$ and $\varepsilon_{r,shell}$ for a fixed measuring distance (z=20 nm) and four different tip radii (R=50, 100, 150 and 250 nm) and in Figure 7.12b where we

show it for a given tip radius (R=100 nm) and different distances z=20, 50 and 100 nm). The electric force (capacitance gradient) depends strongly on both parameters as shown in Figure 7.12c and Figure 7.12d; but this is taken into account by the procedure for extracting $\varepsilon_{r,eff}$.

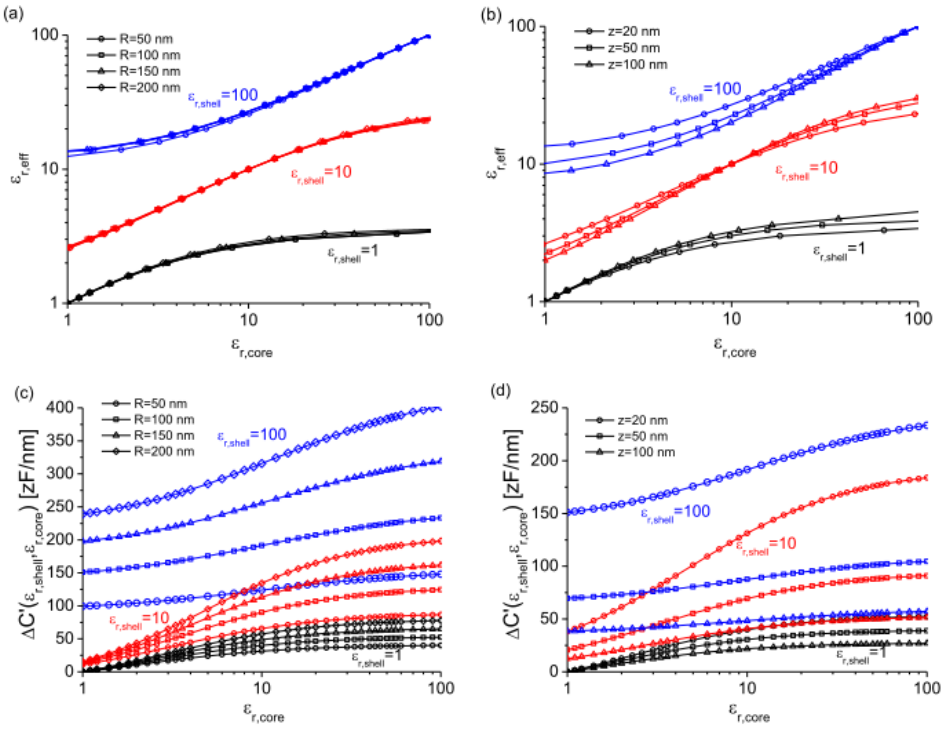

Figure 7.12 *(a&b) Effective dielectric constant and (c&d) capacitance gradient of a core-shell spheroid in an EFM set up as a function of the dielectric constant of the core and for different dielectric constants of the shell, for (a&c) different tip radii R=50 nm-200 nm at fixed tip sample distance z=20 nm and (b&d) different tip sample distances z=20nm-100 nm for a given tip apex radius R=100 nm. Geometric parameters of the cell model correspond to the L. sakei bacteria ($a_{cx} = a_{cy}$ =1.04 μm $\neq a_{cz}$ =0.26 μm, and $a_{sx} = a_{sy}$ =1.1 μm $\neq a_{sz}$ =0.32 μm). Remaining probe parameters: θ=30º and H=15 μm.*